JGR Space Physics

RESEARCH ARTICLE
10.1029/2023JA031494

Special Section:
Fifteen Years of THEMIS Mission

Solar Wind Parameters Influencing Magnetosheath Jet Formation: Low and High IMF Cone Angle Regimes

Laura Vuorinen[1], Heli Hietala[1,2,3], Adrian T. LaMoury[2], and Ferdinand Plaschke[4]

[1]Department of Physics and Astronomy, University of Turku, Turku, Finland, [2]Blackett Laboratory, Imperial College London, London, UK, [3]Department of Physics and Astronomy, Queen Mary University of London, London, UK, [4]Institut für Geophysik und extraterrestrische Physik, TU Braunschweig, Braunschweig, Germany

Key Points:

- Jet formation is sensitive to SW parameters during high interplanetary magnetic field cone angles (quasi-⊥), but not during low cone angles (quasi-∥)
- Quasi-∥ (quasi-⊥) jets have an intrinsic size of ~0.3 R_E (~0.1 R_E) parallel to flow
- Quasi-⊥ jet formation is related to shock dynamics amplified by higher β and M_A

Correspondence to:
L. Vuorinen,
laura.k.vuorinen@utu.fi

Citation:
Vuorinen, L., Hietala, H., LaMoury, A. T., & Plaschke, F. (2023). Solar wind parameters influencing magnetosheath jet formation: Low and high IMF cone angle regimes. *Journal of Geophysical Research: Space Physics*, *128*, e2023JA031494. https://doi.org/10.1029/2023JA031494

Received 17 MAR 2023
Accepted 28 SEP 2023

Abstract Magnetosheath jets are localized flows of enhanced dynamic pressure that are frequently observed downstream of the Earth's bow shock. They are significantly more likely to occur downstream of the quasi-parallel shock than the quasi-perpendicular shock. However, as the quasi-perpendicular geometry is a more common configuration at the Earth's subsolar bow shock, quasi-perpendicular jets comprise a significant fraction of the observed jets. We study the influence of solar wind conditions on jet formation by looking separately at jets during low and high interplanetary magnetic field (IMF) cone angles. According to our results, jet formation commences when Alfvén Mach number $M_A \gtrsim 5$. We find that during low IMF cone angles (downstream of the quasi-parallel shock) other solar wind parameters do not influence jet occurrence. However, during high IMF cone angles (downstream of the quasi-perpendicular shock) jet occurrence is higher during low IMF magnitude, low density, high plasma beta (β), and high M_A conditions. The distribution of quasi-parallel (quasi-perpendicular) jet sizes parallel to flow peaks at ~0.3 R_E (~0.1 R_E). Some quasi-perpendicular jets formed during high β and M_A are particularly small. We show two examples of high β and M_A quasi-perpendicular shock crossings. Jets were observed in the transition region, but not deeper in the magnetosheath. A more detailed look into one jet revealed signatures of gyrating ions, indicating that gyrobunched ions near the shock may produce jet-like enhancements. Our results suggest that jets form as part of the quasi-perpendicular shock dynamics amplified by high solar wind M_A and β.

1. Introduction

Magnetosheath jets are dynamic pressure enhancements that sporadically emerge from the Earth's bow shock and are then observed in the magnetosheath (see the review by Plaschke et al., 2018, and the references therein). These are very common structures as one satellite can observe them many times per hour. Their sizes vary with the largest ones being comparable to the size of the Earth (Plaschke et al., 2016, 2020). Many studies have linked jets to low interplanetary magnetic field (IMF) cone angle (the acute angle between the Sun-Earth line and the magnetic field) conditions (e.g., Archer & Horbury, 2013; LaMoury et al., 2021; Plaschke et al., 2013; Vuorinen et al., 2019). At the subsolar magnetosheath, the cone angle approximates the nominal θ_{Bn} at the bow shock, as the curvature of the shock is small in this region. Thus, these results imply that jets are most frequent when the subsolar magnetosheath is downstream of a quasi-parallel bow shock region.

This trend in jet occurrence has implications for jet formation mechanisms — namely that they are most likely related to the nature of the quasi-parallel shock and to the presence of the foreshock. For example, foreshock transients such as short large amplitude magnetic structures (SLAMS; Schwartz, 1991) or foreshock compressive structures (FCS) in general can pass through the bow shock and be observed as dynamic pressure enhancements in the magnetosheath (Karlsson et al., 2015; Palmroth et al., 2018; Suni et al., 2021). In addition, Hietala et al. (2009) and Hietala and Plaschke (2013) argued that jets can emerge from a rippled quasi-parallel shock surface, when solar wind flowing through a ripple is less decelerated than the flow through the surrounding shock area. Jet formation associated with bow shock ripples has been observed in simulations of a global hybrid model by Karimabadi et al. (2014) and of a local hybrid model by Hao et al. (2016). Recently, Raptis, Karlsson, Vaivads, Pollock, et al. (2022) showed direct evidence of a jet forming during the reformation process of the quasi-parallel shock, as solar wind was trapped downstream between the old and newly-forming shock surface. A minority of jets can also be attributed to solar wind discontinuities interacting with the Earth's bow shock (Archer et al., 2012).

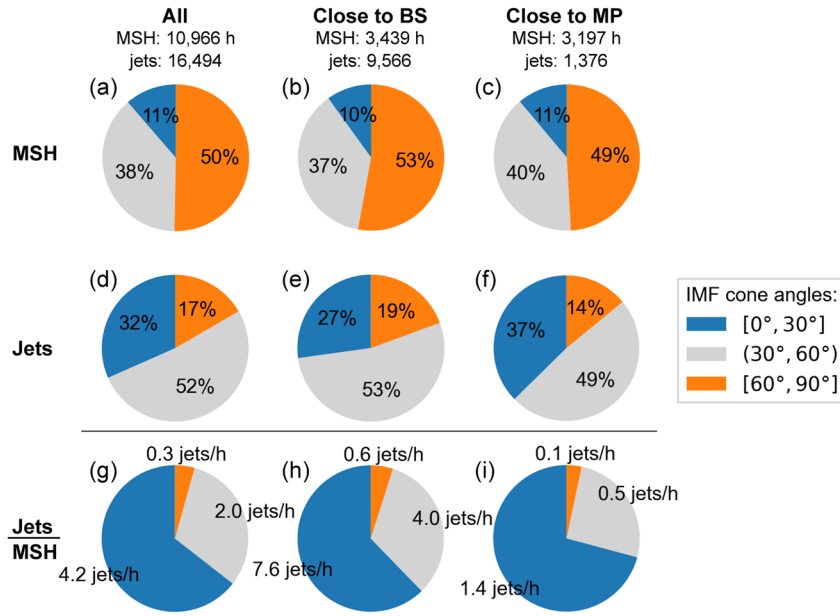

Figure 1. Percentages of the THEMIS (a–c) magnetosheath (MSH) observations and (d–f) jet observations in the three different interplanetary magnetic field cone angle bins. Panels (g–i) show the average number of observed jets per hour of magnetosheath observations. The left-most column (a, d, g) uses all MSH and jet data, the middle column (b, e, h) includes only data close to the bow shock ($F \geq 0.5$), and the right-most column (c, f, i) only data close to the magnetopause ($F \leq 0.25$).

A non-negligible fraction of jets do occur during high IMF cone angles downstream of the quasi-perpendicular shock. The quasi-perpendicular geometry is in fact a much more common configuration for the subsolar bow shock (see Figure 1a introduced in Section 2). This results in the number of jets downstream of quasi-parallel and quasi-perpendicular shocks being more comparable in data sets consisting of many years of dayside magnetosheath observations (see Figure 1). Interplanetary shocks at 1 AU and planetary bow shocks beyond Earth are also frequently quasi-perpendicular. More attention has been recently paid to these jets in the quasi-perpendicular magnetosheath. Raptis et al. (2020) studied jets (enhancements of total dynamic pressure) in the quasi-perpendicular magnetosheath along with quasi-parallel and boundary jets (between the two regimes). They divided these jets downstream of the quasi-perpendicular shock into two categories: quasi-perpendicular jets and encapsulated jets (jets which look like quasi-parallel jets but are observed in the quasi-perpendicular magnetosheath). They argued that encapsulated jets are most likely formed at the quasi-parallel shock but they travel in the magnetosheath and can later be observed in the quasi-perpendicular region. Raptis et al. (2020) found quasi-perpendicular jets to be shorter in duration and weaker in speed, density, and dynamic pressure. Kajdič et al. (2021) studied total dynamic pressure enhancements in the quasi-perpendicular magnetosheath and reported four different types of events, which resulted in jet-like enhancements: reconnection exhausts, magnetic flux tubes connected to the quasi-parallel shock, mirror-mode waves, and non-reconnecting current sheets. Overall, the knowledge of how quasi-perpendicular jets form is still very poor. While it is believed that at the quasi-parallel shock rippling (Hietala et al., 2009; Hietala & Plaschke, 2013) and shock reformation (Raptis et al., 2020) can lead to jet formation, it is not clear whether these or similar mechanisms can lead to jets also at the quasi-perpendicular shock, where the scales of such processes are typically much smaller.

Understanding how solar wind conditions affect jet formation can help us investigate how they form. The IMF cone angle had long been considered as the only parameter controlling magnetosheath occurrence (e.g., Plaschke et al., 2013). Now that even larger data sets are available, mainly thanks to Time History of Events and Macroscale Interactions during Substorms (THEMIS; Angelopoulos, 2008) and Magnetospheric Multiscale Mission (MMS; Burch et al., 2016) missions' dayside configurations, this picture is becoming more complicated. Recently, LaMoury et al. (2021) studied separately the solar wind conditions affecting the formation of jets and their ability to propagate to the magnetopause by separating the data into regions close to the bow shock and close to the magnetopause. The subset close to the bow shock can be considered to be dominated by formation effects, while the near-magnetopause subset is also affected by propagation effects. They reported that, in addition to IMF

cone angle, the solar wind conditions favorable for jet formation are low IMF strength (B), low density (n), low dynamic pressure (P_{dyn}), high plasma beta (β), and high Alfvén Mach number (M_A). Koller et al. (2022) studied the occurrence of magnetosheath jets during large-scale solar wind structures. They found that jet occurrence was increased by ∼50% during stream-interaction regions and high-speed streams, but decreased by ∼50% during coronal mass ejections' sheath regions and magnetic ejecta. This was attributed to different plasma and magnetic field characteristics of the different large scale structures affecting jet formation.

In this paper, we study the solar wind influence on jet formation in more detail. We focus on jets that are generated at the Earth's bow shock and have a significant earthward velocity component. These jets may have the possibility to impact the magnetopause and consequently perturb the magnetosphere and the ionosphere. In particular, we statistically investigate the two regimes, low and high IMF cone angles, separately, as they are linked to the two well-established distinct shock regimes: quasi-parallel and quasi-perpendicular, respectively. We find that low IMF cone angle jet formation is not controlled by other solar wind parameters, but during high IMF cone angles certain solar wind conditions (e.g., high M_A and β) are more favorable for jet formation. First, we introduce the data and methods applied in this study. Second, we present the statistical results and show examples of jet observations at two quasi-perpendicular shock crossings of different upstream β and M_A conditions. Finally, we discuss the implications and caveats followed by the conclusions of this study.

2. Data and Methods

We investigate subsolar magnetosheath data from the THEMIS probes (Angelopoulos, 2008) from the years 2008–2020. We use data from the Fluxgate Magnetometer (FGM; Auster et al., 2008) and the Electrostatic Analyzer (ESA; McFadden et al., 2008). The statistical data set uses on-board moment data and all observations have been interpolated to a common 1-s cadence. This is a relevant step to note when considering jet durations and comparisons with other missions. This particular THEMIS magnetosheath and jet data set has been created using the algorithm presented by Plaschke et al. (2013) (see their paper for details) and was first used by Koller et al. (2022). It is publicly available (Koller et al., 2021). The solar wind conditions for each of the magnetosheath (and jet) measurements are obtained from the OMNI high-resolution 1-min data set (J. H. King & Papitashvili, 2005). However, we apply a running average of the five preceding minutes to obtain a more reliable estimate of the general solar wind conditions at the time of jet formation. The Plaschke et al. (2013) algorithm selects for THEMIS data within a 30° cone around the Sun-Earth line, within geocentric distances of 7–18 R_E. To exclude solar wind and inner-magnetospheric observations, they included two constraints: (a) the ion density has to exceed twice that of the solar wind, and (b) the energy flux of 1 keV ions has to exceed that of 10 keV ions. At the end of this paper, we present a few examples of shock crossings. In these examples, we use THEMIS ground data (available during fast survey mode intervals).

The main jet criterion is that at some point in a magnetosheath jet, the earthward dynamic pressure has to exceed half of the solar wind dynamic pressure. The jet interval is defined as the period when the earthward dynamic pressure in the magnetosheath is larger than one quarter of the solar wind dynamic pressure. At some point within 1-min intervals both before and after the jet interval, V_X (in GSE coordinates) in the magnetosheath has to exceed $V_X(t_0)/2$ (t_0 is the time when the dynamic pressure ratio reaches its peak within the jet). This ensures that jets exhibit an increase in earthward flow speed. Note that this criterion means that not every enhancement of dynamic pressure is considered a jet. The measurements at t_0 of each jet represent the jet observations in our statistical study.

As demonstrated by LaMoury et al. (2021), it is important to disentangle solar wind influence on jet formation and jet propagation. Thus, we only use data from the outermost half of the magnetosheath close to the bow shock to remove effects of propagation. We select the data by assigning each THEMIS observation a relative radial position F in the magnetosheath (magnetopause at $F = 0$ and bow shock at $F = 1$)

$$F = (r - r_{MP})/(r_{BS} - r_{MP}) \quad (1)$$

by applying Shue et al. (1998) magnetopause model and Merka et al. (2005) bow shock model. Here r is the geocentric distance of the spacecraft. r_{BS} and r_{MP} are the geocentric distances of the model bow shock and magnetopause, respectively, measured along the line connecting the spacecraft and the center of the Earth. We use the constraint $F \in [0.5, 1.1]$, because we want to maximize the number of observations to obtain the best possible statistics. The jet occurrence has not decreased significantly before half-way ($F = 0.5$) through the magnetosheath

(not shown here, but can be seen in Figure 1 of LaMoury et al., 2021), implying that propagation effects are not yet significant. There are uncertainties both in the bow shock and magnetopause models and in the OMNI data, which is why we accept values up to $F = 1.1$, where the jet occurrence quickly decreases.

In order to study the quasi-parallel and quasi-perpendicular regimes separately, we divide the observations by the IMF cone angle

$$\alpha = \arccos(|B_X|/B) \in [0°, 90°], \tag{2}$$

where B_X is the X component of the magnetic field vector in GSE coordinates. The cone angle distributions of jet and magnetosheath (MSH) observations of the data set are shown in Figure 1 for the whole data set and also separately for observations close to the model bow shock and close to the model magnetopause. Quasi-parallel (quasi-perpendicular) regime is represented by low (high) cone angles $\leq 30°$ ($\geq 60°$). Vuorinen et al. (2019) showed that for these extreme ranges of cone angles, the jet occurrence rates are spatially uniform in the subsolar region. For the intermediate values (30°, 60°), one part of the subsolar magnetosheath is downstream of the quasi-parallel and the other downstream of the quasi-perpendicular shock, and thus the jet occurrence rate varies spatially. To clearly separate these two regimes, we exclude the data with such intermediate cone angles. Figure 1 displays that close to the bow shock, where we are focusing on in this study, 27% of jets in the THEMIS data occurred during low IMF cone angles and 19% occurred during high IMF cone angles. In contrast, only 10% of MSH observations were taken during low IMF cone angle conditions and 53% during high IMF cone angles. This illustrates that jets are much more common during low IMF cone angles, but as high IMF cone angle conditions are more frequent at Earth, quasi-perpendicular jets make up a significant portion of jets in the Earth's magnetosheath.

We apply Bayes' theorem

$$P(\text{jet}|\text{conditions}) = \frac{P(\text{conditions}|\text{jet})P(\text{jet})}{P(\text{conditions})} \tag{3}$$

to calculate conditional probabilities, that is, normalized jet occurrence rates under different solar wind conditions. The probabilities on the right-hand side of the equation can be estimated using the observations: $P(\text{jet}) = N_{\text{jet}}/N_{\text{msh}}$, $P(\text{conditions}) = N_{\text{msh}}(\text{conditions})/N_{\text{msh}}$, and $P(\text{conditions}|\text{jet}) = N_{\text{jet}}(\text{conditions})/N_{\text{jet}}$. Thus, the equation becomes

$$P(\text{jet}|\text{conditions}) = \frac{N_{\text{jet}}(\text{conditions})}{N_{\text{msh}}(\text{conditions})}. \tag{4}$$

Because jets are mostly observed during smaller cone angles but higher cone angles are more frequent in the whole magnetosheath data set, without the separation by IMF cone angles we would be generally comparing jets and magnetosheath observations during very different IMF cone angle conditions. Low and high IMF cone angle solar wind have statistically different distributions in other parameters (not shown here). This means that without taking the IMF cone angle into account in the normalization, the normalized occurrence rates can just reflect the differences between low and high IMF cone angle solar wind conditions. In high-dimensional data sets, it can be difficult to account for all the interdependencies of different parameters. However, classifying the data with the IMF cone angle is important and meaningful as there are very strong differences in IMF cone angle distributions between jet and MSH data sets, and quasi-parallel and quasi-perpendicular shock regimes are well-established and known to be different.

3. Results

3.1. THEMIS Statistical Results

In Figure 2, we present the normalized distributions of jet occurrence as a function of the OMNI solar wind parameters. For the derived parameters, we use the definitions and values used in the high-resolution OMNI data set itself (see J. King et al., 2023, https://omniweb.gsfc.nasa.gov/html/omni_min_data.html#4b, and https://omniweb.gsfc.nasa.gov/ftpbrowser/bow_derivation.html for the detailed derivations). The blue histograms represent low IMF cone angles ($\leq 30°$) and the orange histograms represent high IMF cone angles ($\geq 60°$). There seems to be a threshold for jet formation, as it is effectively suppressed for very low $\beta \lesssim 0.5$ and $M_A \lesssim 5$ conditions for both quasi-parallel and quasi-perpendicular regimes. However, during low IMF cone angle conditions, there are only 2–3 hr of magnetosheath data in these low β and M_A bins. Overall, we can see that for low IMF cone angles (downstream of the quasi-parallel shock), the distributions are relatively flat (within error bars), while there are clear trends in many distributions for high IMF cone angles. A flat histogram indicates that the parameter has no

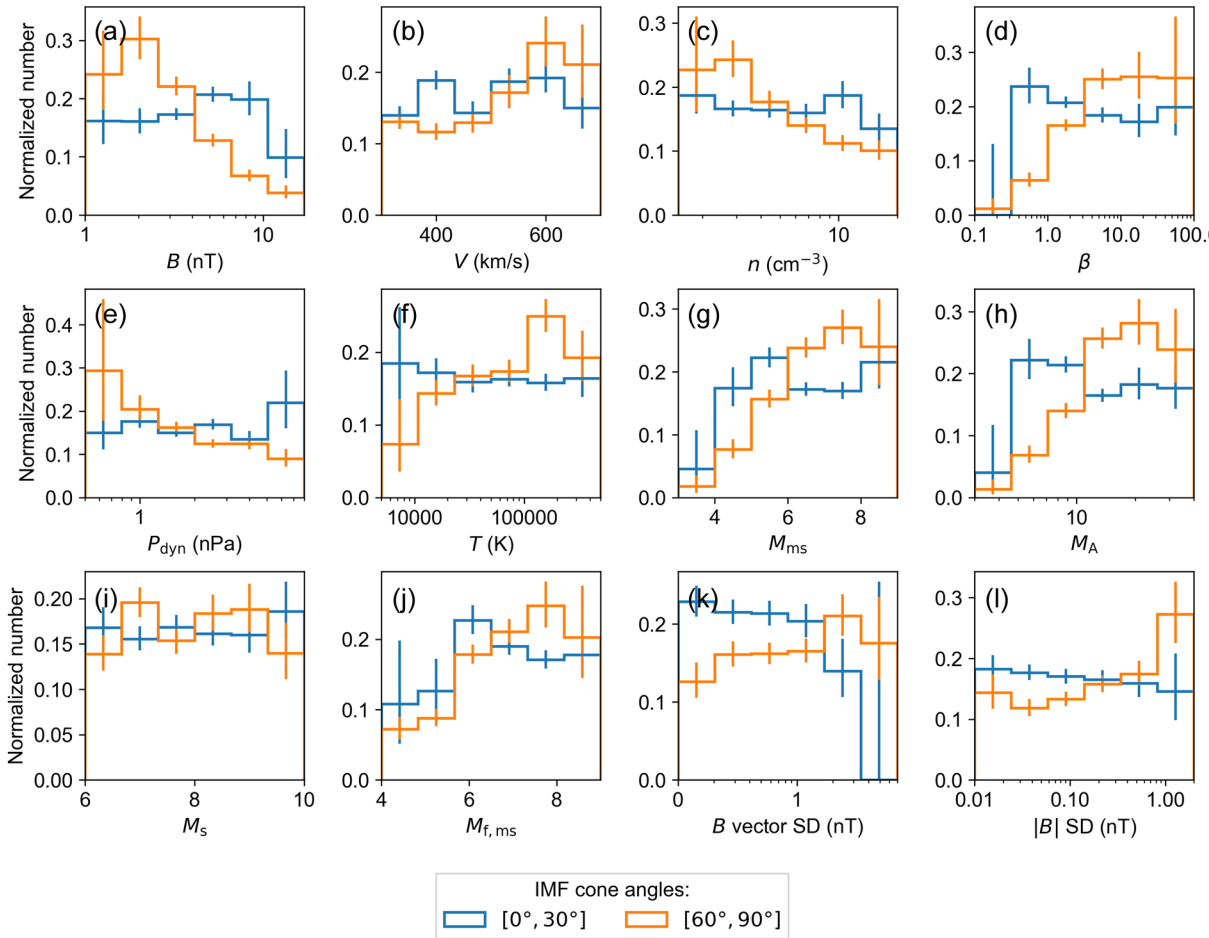

Figure 2. Distributions showing the normalized occurrence rates of jets (jets distribution normalized by the magnetosheath distribution) as functions of OMNI interplanetary magnetic field (IMF) and solar wind parameters: (a) IMF magnitude, (b) speed, (c) density, (d) β, (e) dynamic pressure, (f) ion temperature, (g) magnetosonic Mach number, (h) Alfvén Mach number, (i) sonic Mach number, (j) fast magnetosonic Mach number, (k) IMF vector standard deviation, and (l) IMF magnitude standard deviation. The distributions are shown separately for observations during low ([0°, 30°]; blue) and high IMF cone angles ([60°, 90°]; orange). The error bars denote 95% proportional confidence intervals.

influence on jet formation, as we see no preference in the data for any particular values. However, trends in the histograms indicate that there is a preference, that is, jets are more often observed during certain solar wind conditions. The results indicate that conditions favorable for jet formation during high IMF cone angles (downstream of the quasi-perpendicular shock) are especially: low B, low n, high β, and high Mach numbers (except for sonic Mach number). Also low P_{dyn}, high V, and high T seem to be favorable for quasi-perpendicular jet occurrence. Although not shown here, similar results for solar wind conditions are obtained when looking at short- and long-duration jets separately.

In Figure 3, we show the distributions of jet durations, lengths parallel to the jet propagation direction $\mathbf{v}(t_0)$, and the ratio of jet and solar wind earthward dynamic pressure for low (blue solid line) and high (orange solid line) IMF cone angles separately. During high IMF cone angles, the jets tend to be clearly smaller (both in duration and parallel length; Figures 3a and 3b). The quasi-perpendicular jet size distribution peaks at ∼0.1 R_E. Small jets are much less common during low IMF cone angles, and the size distribution of quasi-parallel jets peaks at ∼15 s and ∼0.3 R_E. Jets are also weaker during high IMF cone angles as can been in Figure 3c. We have additionally included the histograms representing jets observed during high IMF cone angle and $\beta < 2$ conditions. We can see that for parallel lengths, this histogram is more similar to the distribution of jets during low IMF cone angles. This shows that for high IMF cone angle conditions or the quasi-perpendicular shock, high $\beta > 2$ (or high M_A, although not shown here) in particular increases the formation of small jets. This does not account for the whole difference

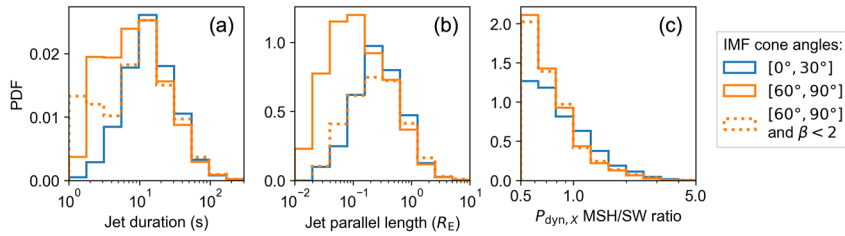

Figure 3. Distributions of (a) jet duration, (b) jet length parallel to $\mathbf{v}(t_0)$, and (c) $P_{\mathrm{dyn},X}$ ratio between the jet value and the solar wind value at t_0. The distributions are shown separately for low interplanetary magnetic field (IMF) cone angles (solid blue), high IMF cone angles (solid orange), and high IMF cone angles with SW $\beta < 2$ (dotted orange).

in jet occurrence rates for low and high β, as jets of all sizes are more common during high β. There is no such difference in the distributions of jet strengths (jet/SW dynamic pressure ratios) between low and high β conditions.

3.2. Examples of Quasi-Perpendicular Bow Shock Crossings During Different β and M_A Conditions

To better understand the statistical results for jets during high IMF cone angles, we present examples of quasi-perpendicular shock crossings observed by THEMIS during different solar wind β and M_A conditions. We show two events, which show us how the structure of the shock changes with increasing β and M_A, and how that relates to observations of downstream jets. We move from low to high β and M_A. We use the Plaschke et al. (2013) jet algorithm to look for jets in the data. The events are THEMIS multi-spacecraft events, in which we can confirm the quasi-perpendicular geometry and β and M_A conditions with simultaneous local upstream measurements instead of relying only on OMNI measurements.

First, we look at Event 1 observations by THEMIS A, D, and E spacecraft on 11 May 2015, around ~21:00 UT. The spacecraft were all located near the bow shock nose. These locations are shown in Figures 4c and 4d. THEMIS A was in the solar wind, THEMIS E crossed the bow shock from the magnetosheath to the solar wind, and THEMIS D was in the magnetosheath (see Figure 4). Figures 4c and 4d also show a model bow shock shape (Merka et al., 2005) and the estimated bow shock normal at the point closest to THEMIS E. We have plotted the average magnetic field vectors during 20:57–21:02 UT measured by OMNI and by THEMIS A in the solar wind. We see that the bow shock was clearly very perpendicular: $\theta_{Bn} = 84°$ based on THEMIS A observations and $\theta_{Bn} = 89°$ based on OMNI observations. The solar wind β and M_A were, respectively, 5.5 and 16 according to OMNI (Figures 4a and 4b) and 2.4 and 8.5 according to local THEMIS A observations in the upstream. We note that temperature observations of THEMIS ESA instrument can be unreliable in the solar wind due to the narrowness of the solar wind beam, and thus there is uncertainty especially in β.

Figures 4e–4k show the measurements from these three locations. THEMIS A observes no foreshock and quite steady solar wind. Nearby THEMIS E crosses from the magnetosheath into the solar wind with a shock transition region in between. This transition region is structured with more variations in magnetic field, density, and velocity compared the magnetosheath proper that was observed before. The separations of different spacecraft at the time that THEMIS E enters or at the time that it exits the transition region sets an upper limit of ~1, 500 km for the width of the this region. Two 10–20 s and three smaller jets can be identified within this transition region. The two largest jets are 1,900 km (the first jet) and 1,000 km (the second jet) in length parallel to their flow direction, which correspond to 26 and 14 upstream ion inertial lengths (with upstream number density 10 cm^{-3}), respectively. THEMIS D further in the magnetosheath observes the much less structured and higher temperature magnetosheath proper. Figure 5 is a zoom-in of THEMIS E observations during the quasi-perpendicular transition region. Here the data are interpolated to 1 s cadence to be comparable with the statistical data set. Note that changing the cadence of the data slightly changes the lengths of the jet intervals. The first two jets exhibit significant increases in earthward flow velocity, while the other jets are driven by density increases. The first jet is a strong one in terms of its earthward dynamic pressure ratio (~90%) while the others are weak. Burst-mode data are not available, but the reduced-mode data reveal a complex multi-population ion distribution around the first jet (not shown).

Next, let us look at Event 2 observations by THEMIS B and C on 10 August 2009, around ~20:10 UT. Figures 6c and 6d show the positions of the spacecraft, and the observed magnetic field orientations by OMNI and THEMIS C in the solar wind at 20:10–20:15. Figures 6e–6k show the observations of THEMIS C in the upstream and THEMIS B crossing the bow shock from the magnetosheath to the solar wind. The solar wind β and M_A were,

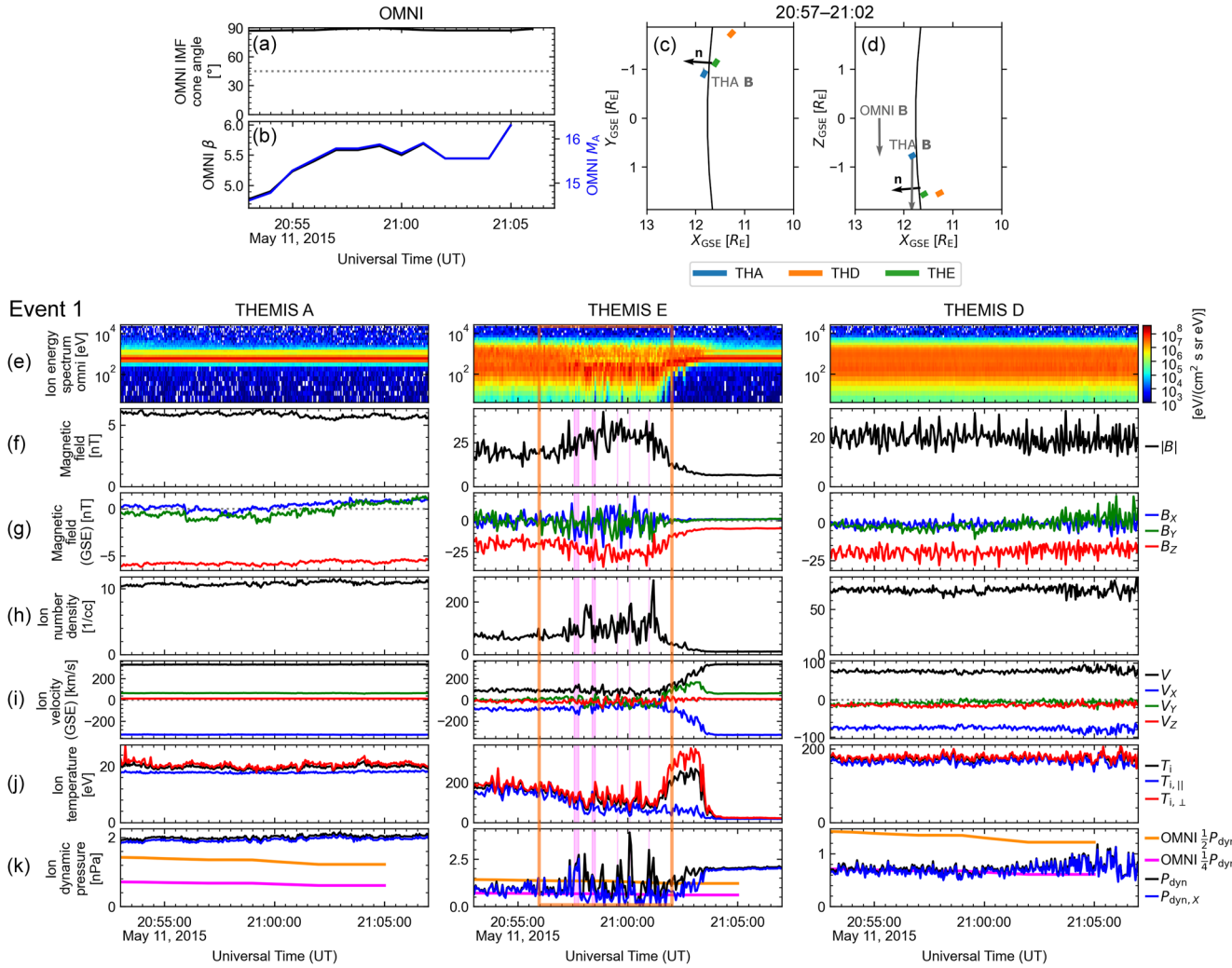

Figure 4. OMNI measurements for Event 1 on 11 May 2015: (a) interplanetary magnetic field cone angle, (b) β and M_A. The locations of THEMIS A, D, and E spacecraft during 20:57–21:02 UT in the GSE (c) X–Y plane and (d) X–Z plane. The black line represents a model bow shock (Merka et al., 2005). The black arrows represent the model bow shock normal vectors at the point closest to THEMIS E. Gray arrows represent the average magnetic field vectors observed by OMNI and THEMIS A in the solar wind. THEMIS A, E, and D observations: (e) ion omni-directional energy spectrogram, (f) magnetic field magnitude, (g) magnetic field in GSE, (h) ion number density, (i) ion velocity in GSE, (j) ion total, parallel, and perpendicular temperatures, and (k) total and GSE $-X$ aligned dynamic pressures with 1/2 (orange) and 1/4 (magenta) of OMNI solar wind dynamic pressure. The magenta shading indicates a jet found using the Plaschke et al. (2013) jet criterion on reduced level ESA data.

respectively, 170 and 93 according to OMNI (Figures 6a and 6b) and 100 and 55 according to local THEMIS C observations in the upstream. The IMF magnitude is remarkably low in this event, as THEMIS C is observing B ~1 nT. Because the M_A is so extremely high, the Merka et al. (2005) bow shock model does not produce realistic bow shock shape anymore (in Figures 6c and 6d we have plotted a model bow shock shape with a higher magnetic field magnitude $B = 2$ nT for illustration). However, we can estimate θ_{Bn} with the IMF cone angle. OMNI measurements yield an IMF cone angle of 86° and the local THEMIS C observations yield the same value. As the THEMIS B and C spacecraft are observing the subsolar region, θ_{Bn} has to be very high with this perpendicular field. The lack of >10 keV ions in the ion energy spectrogram is again consistent with this.

While THEMIS C observes relatively steady upstream conditions, THEMIS B crossing the bow shock observes a prolonged transition of magnetosheath plasma to the solar wind plasma (Figures 6e–6k). This shock crossing exhibits a train of high-amplitude magnetic field enhancements in the upstream region, which grow larger toward the shock. Note the arrow on the top of the THEMIS B panel, which indicates the beginning of the magnetosheath interval in which we search for jets. One very short-duration jet and two ~20 s jets can be identified within this interval with the ground reduced ESA data. The sizes of the largest jets are 2,100 km

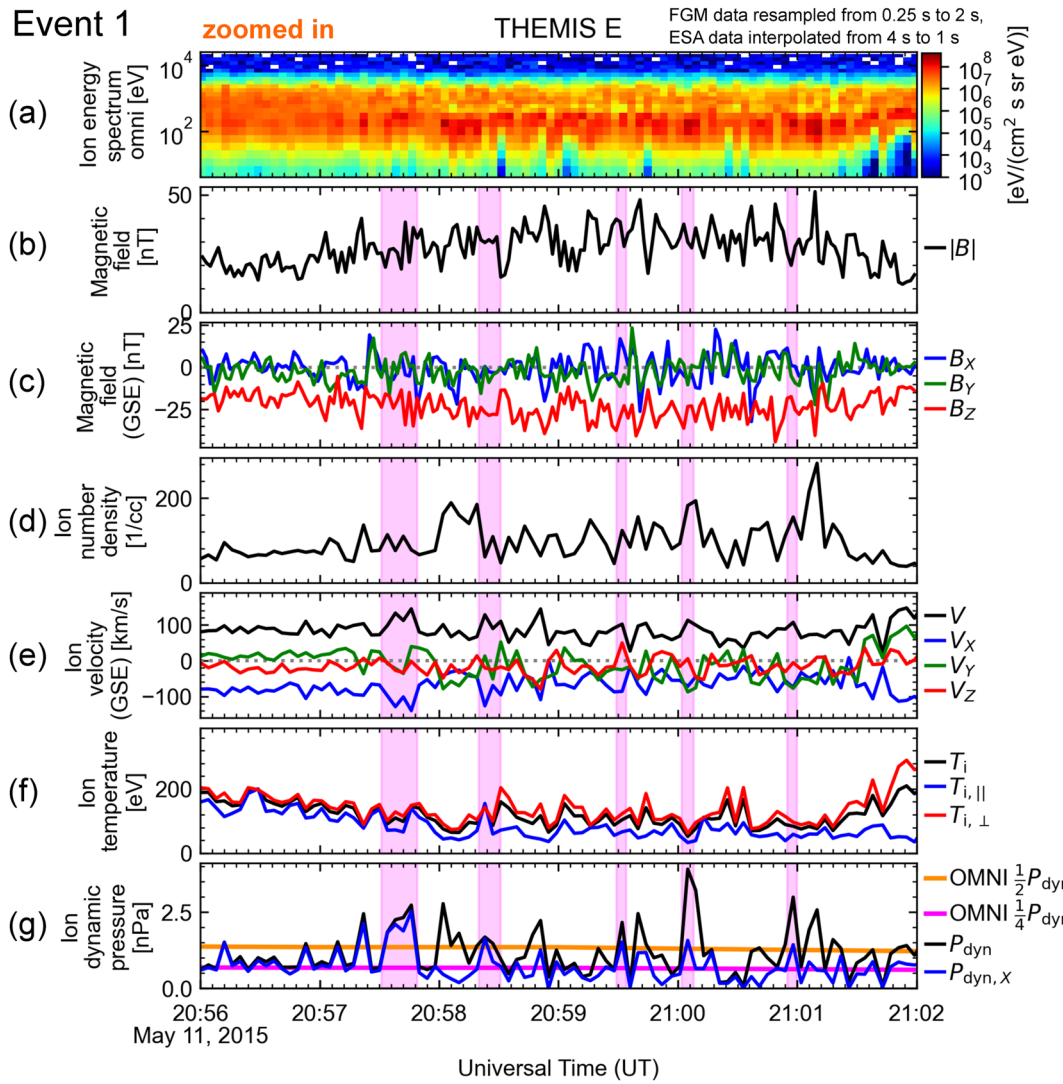

Figure 5. A zoom-in of THEMIS E observations for Event 1 in the same format as in Figures 4e–4k. The plasma data have been interpolated to 1 s cadence to match the cadence of the statistical data set. The magenta shading indicates a jet found using the Plaschke et al. (2013) jet criterion on this 1-s cadence data.

(the second jet) and 2,200 km (the third jet), which correspond to 21 and 22 upstream ion inertial lengths (with upstream number density 5 cm^{-3}). Figure 7 shows a zoom-in to THEMIS B observations downstream during 20:09:20–21:15:20 UT. In this interval, right downstream of the shock, the flow velocity has already decreased substantially and the density has increased, but there are still high-amplitude variations in magnetic field and density. The second jet exhibits a high increase in earthward velocity. Figure 7h presents V_X-V_Y slices of the ion distribution burst-mode data (averaged over [−20°, 20°] in elevation from the $V_Z = 0$ plane) around this jet. Note that the upstream magnetic field is approximately in the −Z-direction, while the magnetic field is highly varying in the downstream region. Figure 7i shows the same slices multiplied by a factor $V_X^2 + V_Y^2$ to represent contribution to dynamic pressure. These plots show signatures of ion gyration and possibly reflection off of magnetic enhancements present in the magnetosheath. At the time of the jet, the gyration seems to be contribute to the increase in earthward dynamic pressure. Before this zoom-in window of Figure 7, THEMIS B observes magnetosheath with less variations and higher temperature (see Figures 6e–6k). We again interpret this as the shock having a structured transition layer, which also contains jets, and deeper in the magnetosheath these variations have dissipated.

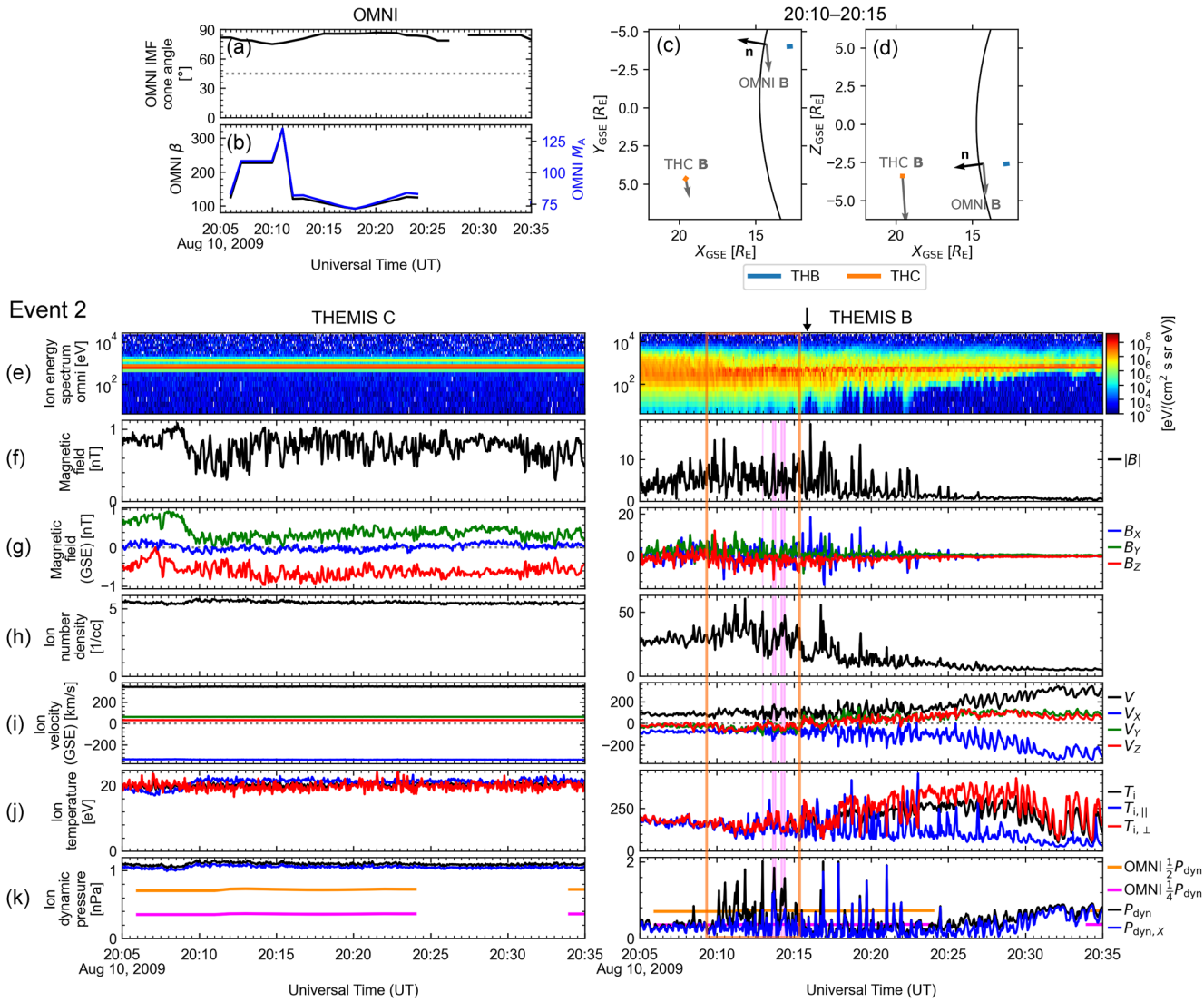

Figure 6. (a, b) OMNI measurements for Event 2 on 10 August 2009, (c, d) the locations of THEMIS B and C spacecraft during 20:10–20:15 UT, and (e–k) THEMIS C and B observations. In the same format as in Figure 4. The magenta shading indicates a jet found using the Plaschke et al. (2013) jet criterion on the ESA reduced level data. The black arrow on top shows the selected upstream edge of the magnetosheath window in which we search for jets. The model bow shock (Merka et al., 2005) shown for reference is calculated for $B = 2$ nT, as the model is not reliable for the observed values $B \lesssim 1$ nT.

4. Discussion

On top of the now well-established link between jets and low IMF cone angles, or the quasi-parallel shock, LaMoury et al. (2021) found additional parameters affecting jet formation. They concluded that low B, low n, high β, and high M_A are favorable conditions for jet generation. According to our detailed study, these results apply to jets forming during high IMF cone angle conditions. During low IMF cone angles, other solar wind parameters do not have a significant influence on jet occurrence. However, jet occurrence is very effectively suppressed for very low $\beta \lesssim 0.5$ and $M_A \lesssim 5$ conditions for both quasi-parallel and quasi-perpendicular regimes (although there is statistical uncertainty for the quasi-parallel case). This corresponds relatively well with the threshold ($M_A \sim 2$–3) where the shock becomes subcritical and ceases to reflect particles (Burgess et al., 2012; Kennel et al., 1985). In other words, substantial ion reflection is most likely a key ingredient for jet formation, as it strongly influences the structure and dynamics of both quasi-parallel (see, e.g., Burgess et al., 1989, 2005) and quasi-perpendicular shocks (see, e.g., Bale et al., 2005; Scholer et al., 1993). This is in line with suggested jet formation mechanisms at the quasi-parallel shock: bow shock ripples (Hietala et al., 2009), cyclic reformation (Raptis, Karlsson, Vaivads, Pollock, et al., 2022), and FCS (Suni et al., 2021), which are inherently related to

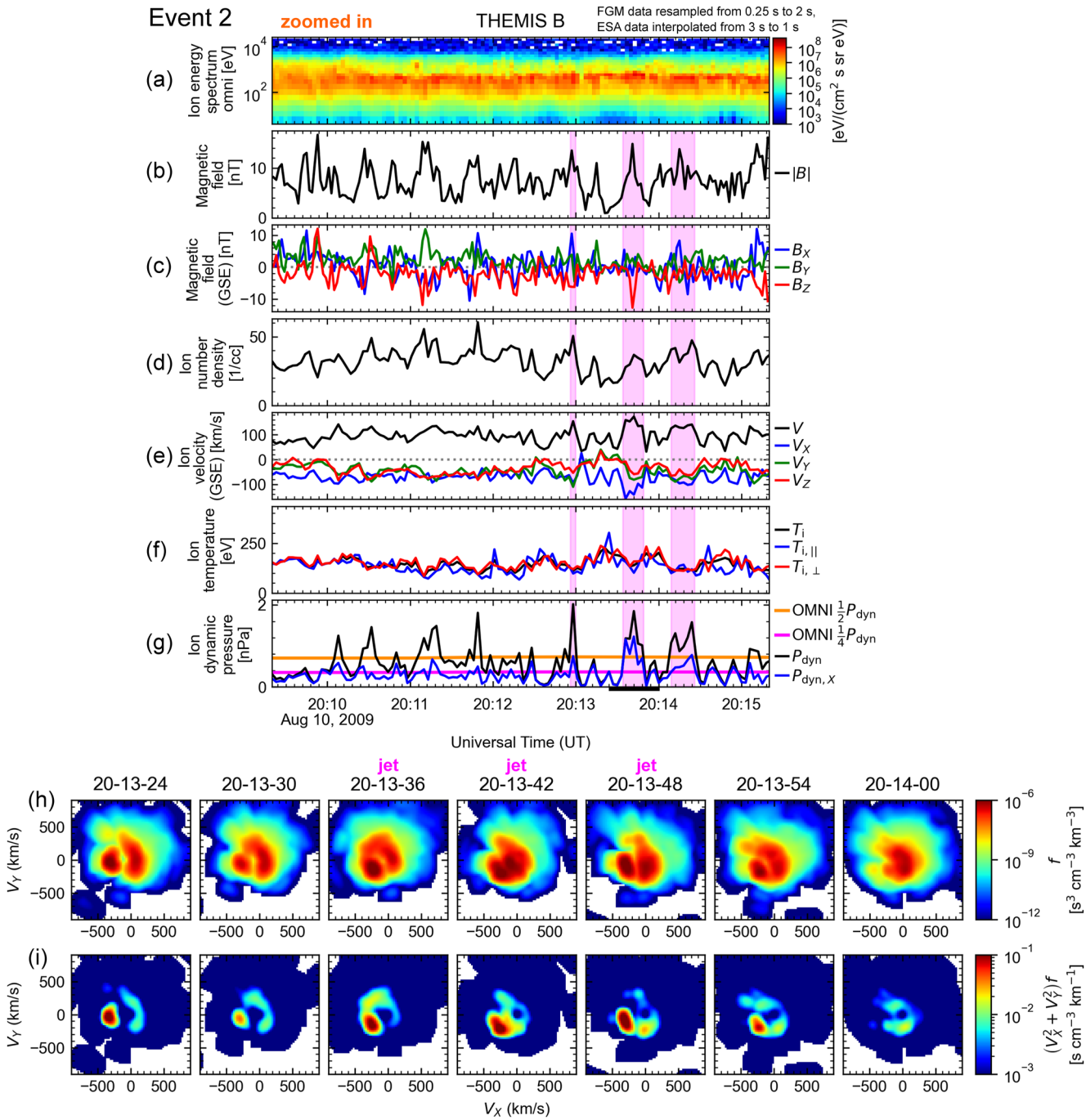

Figure 7. (a–g) A zoom-in of THEMIS B observations for Event 2 in the same format as in Figure 5. The plasma data have been interpolated to 1 s cadence to match the cadence of the statistical data set. The magenta shading indicates a jet found using the Plaschke et al. (2013) jet criterion on this 1-s cadence data. (h) V_X-V_Y slices of the ion distribution function at selected timestamps (the window is highlighted with a black bar at the bottom of panel g). (i) The slices multiplied by a factor $V_X^2 + V_Y^2$.

the foreshock ULF wave field. Tinoco-Arenas et al. (2022) studied 2D local hybrid simulations of shocks with parameters close to these threshold values. They used $\beta = 0.5$ and varied θ_{Bn} and M_A. They found jets within the whole parameter range $M_A \in [4.28, 7.42]$.

Separating the data to low and high IMF cone angles is important as most jets are observed during lower IMF cone angles and most magnetosheath measurements are made during higher cone angles. Thus, when normalizing the jet data by the magnetosheath data (i.e., calculating conditional probabilities; Equation 4) without this distinction

(as in LaMoury et al., 2021), the results will be exhibiting differences in solar wind characteristics during low and high IMF cone angles rather than only in jet occurrence rates. Classifying the data by cone angles removes this effect and allows us to better compare the occurrence rates during different solar wind conditions. Goncharov et al. (2020) also studied jets in the quasi-parallel and quasi-perpendicular dayside magnetosheath, including flank observations, with slightly different jet criteria and a smaller MMS data set. They did not normalize for relative radial position in the magnetosheath, that is, separate formation and propagation. They also did not separate the normalizing magnetosheath data into these two regimes, which we argue is important because otherwise we end up comparing lower IMF cone angle jet observations mostly to higher IMF cone angle magnetosheath observations. Their results suggested that jets are more common during higher magnetic field magnitude, solar wind speed, M_A, and β. The last two results are in agreement with our results (but only for the quasi-perpendicular case), but the first two are not. The favorability they observed for higher solar wind speed may be explained by their criterion for higher dynamic pressure jets and by propagation effects (LaMoury et al., 2021). Similarly, high magnetic field magnitude is favorable for jet propagation deep into the magnetosheath. Recently, Koller et al. (2023) used the data set applied in this study to investigate jet occurrence during large-scale solar wind structures. They reported that jet occurrence is very low during high IMF cone angle and low Alfvén Mach number conditions, which makes magnetic clouds of coronal mass ejections unfavorable for jets.

We also statistically studied the durations of jets, their lengths parallel to their propagation direction, and their dynamic pressure ratios (i.e., strengths). We find that the durations of quasi-parallel jets peak at a little more than 10 s duration. This is comparable to the period of ULF waves in the terrestrial ion foreshock. According to our results, quasi-perpendicular jets tend to be smaller than quasi-parallel ones, which agrees with previous studies (e.g., Goncharov et al., 2020; Raptis et al., 2020). We also find that quasi-perpendicular jets tend to have a lower $P_{\mathrm{dyn},X}$ jet/SW ratio, meaning that they are weaker, as also found by Raptis et al. (2020). When taking a low plasma beta subset ($\beta < 2$) of the high IMF cone angle set, we find that they seem to be more similar to low IMF cone angle jets in their size distribution. The high beta quasi-perpendicular subset ($\beta \geq 2$) represents the newly resolved population of the smallest jets. However, jets of all sizes are more common during high β.

While OMNI data allow us to link every magnetosheath observation to a solar wind measurement, this data set is known to contain uncertainty (e.g., Vokhmyanin et al., 2019; Walsh et al., 2019). OMNI data are combined from multiple spacecraft at L1 and then propagated to the Earth's bow shock. While these data are very useful for large statistical studies where errors can be assumed to average out, one cannot blindly trust it when looking at individual events. Because quasi-perpendicular jets have significantly lower occurrence rate than quasi-parallel jets, a number of the high IMF cone angle jets in this data set have most likely been misclassified, and in reality they have formed at the quasi-parallel shock. For individual events, it is important to use local upstream measurements to verify the shock geometry. Similarly, the bow shock model (Merka et al., 2005) and the magnetopause (Shue et al., 1998) model contain uncertainty. We note the models have ranges of solar wind values where they are valid, and thus the leftmost and rightmost bins in Figure 2 are most unreliable in terms of F values. The assumption that data with $F \in [0.5, 1.1]$ are close to the bow shock may therefore not hold in these bins.

We provided two examples of multi-spacecraft quasi-perpendicular shock crossings with different β and M_A to give context on how the quasi-perpendicular shock transition changes with increasing β and M_A and how these dynamics may be linked to jet formation. We used local upstream observations including simultaneous two-point measurements by THEMIS to verify the steady quasi-perpendicular geometry and the high β and M_A in the solar wind. With increasing β and M_A the shock transition becomes more extended. With multi-point observations, we were able to estimate the thickness to be <1, 500 km for the $\beta \sim 5$ event (Event 1). Note, however, that the observed duration depends on the relative motion between the shock and the spacecraft. The so-called transition region exhibits high-amplitude variations particularly in magnetic field magnitude and density. There is no clear anti-correlation between magnetic field magnitude and density, so we do not consider these mirror mode waves, which are typical in the quasi-perpendicular magnetosheath proper. In contrast, the magnetic field and density are often enhanced together. There are also enhancements of dynamic pressure and some of these can be identified as earthward jets by the Plaschke et al. (2013) criterion. These jets are indeed present in the shock transition region but were not recorded in our examples deeper in the magnetosheath. A statistical investigation also revealed that quasi-perpendicular jets during high M_A solar wind conditions typically occur very close to the model bow shock (not shown). Thus, these type of jets are probably not very likely to go on and impact the magnetopause, perhaps as they dissipate in the transition region. In Event 2, burst-mode ion data were available, and we investigated the ion distributions near the strongest and largest jet. Similar to previous observations by Raptis, Karlsson,

Vaivads, Lindberg, et al. (2022), the ion distributions were complex. Ion gyromotion, and possibly reflection off of magnetic structures, was found to contribute to an increase in earthward dynamic pressure.

In 2D hybrid simulations of low to moderate M_A quasi-perpendicular shocks, Ofman and Gedalin (2013) found that the non-gyrotropic gyromotion of directly transmitted protons causes enhancements in bulk speed and dynamic pressure and decreases in magnetic field strength right downstream of the shock. Similarly, McKean et al. (1996) found helium ions to form gyrobunched populations that cause fluctuations downstream. For higher M_A, simulations of McKean et al. (1995) showed that gyrobunched populations of reflected protons (the "ring-beam") may carry substantial energy in the downstream region close to the shock. Non-gyrotropic ion motion close to the shock may thus lead to jet-like observations close to the shock, before the distribution becomes more isotropic further in the downstream.

Previous observations of the Earth's quasi-perpendicular bow shock during high M_A (Madanian et al., 2021; Sundberg et al., 2017) and high β (Petrukovich & Chugunova, 2021) (high M_A and high β are tied to each other at Earth's heliocentric distance) show that such shock crossings are extended and exhibit high magnitude structures both upstream and downstream, most likely related to shock reformation. Sulaiman et al. (2015) studied several high M_A Saturn's bow shock crossings and showed that there is a reformation cycle typically at a period of ∼26% of the ion gyroperiod. Similarly, the quasi-perpendicular shock can also exhibit ripples that move along the shock surface and have similar timescales of ∼0.3–0.4 gyroperiods (Johlander et al., 2016; Lowe & Burgess, 2003). These timescales increase for lower upstream magnetic field magnitude (for higher β and M_A conditions), becoming tens of seconds for IMF $B \lesssim 1$ nT. As quasi-parallel jet formation has been suggested to be related to bow shock rippling (Hietala et al., 2009; Hietala & Plaschke, 2013) and Raptis, Karlsson, Vaivads, Pollock, et al. (2022) showed that quasi-parallel shock reformation can lead to downstream jets, already known, or similar, mechanisms could possibly contribute to jet formation at quasi-perpendicular shocks, as well.

Recently, Omidi et al. (2021) studied the spatial and temporal structure of a high M_A quasi-perpendicular shock with a global 2.5D simulation. Their simulation results indicate that upstream structures, such as previously reported for these type of shocks, can emerge in spacecraft data due to a surface wave moving along a shock and the shock crossing the spacecraft numerous times. These results highlight an important and inherent issue of disentangling temporal and spatial variations when analyzing single-spacecraft data. More detailed multi-spacecraft studies are needed to discard possible misclassifications of bow shock crossings as jets and to study how jets move with respect to the surrounding plasma. We note that the width of the shock transition region, and also the jets within, is dependent on the speed of the spacecraft moving in space and/or on the speed of the shock as it moves across the spacecraft.

Finally, we highlight that the time resolution of observations can have an effect on whether a jet algorithm classifies a certain structure as a jet. Thus, different data sets may yield relatively more or fewer jets due to differences in cadences. This is important to consider when comparing or combining data from different instruments and missions. For example, we have investigated MMS measurements (FPI cadence 150 ms; Pollock et al., 2016) downstream of perpendicular shocks. The Plaschke et al. (2013) algorithm finds very short duration jets when applied to the burst-level data, indicating that such exist, as implied by our statistical results and by the predictions of Plaschke et al. (2020). However, these jets are not found when the data are downsampled to the THEMIS 3 s cadence.

5. Conclusions and Summary

In this study, we have statistically studied how solar wind conditions influence jet occurrence in the two regimes of low and high IMF conditions using an extensive THEMIS spacecraft data set from the years 2008–2020. This allows us to better understand jet formation at the quasi-parallel and quasi-perpendicular shocks, respectively. Jet formation is observed to commence for $\beta \gtrsim 0.5$ and $M_A \gtrsim 5$ for both shock geometries. We found that during low IMF cone angles, jet occurrence close to the bow shock is not sensitive to the other solar wind parameters. In contrast, during high IMF cone angle conditions, jet formation changes as a function of other solar wind parameters: quasi-perpendicular jets are more frequently observed when the IMF magnitude is low, the SW speed is high, the SW density is low, the plasma beta is high, and the Alfvén Mach number is high. The quasi-parallel jets have an intrinsic scale size: the distribution of sizes (parallel to flow) peaks at ∼15 s and ∼0.3 R_E. The jets formed during high IMF cone angles (or at the quasi-perpendicular shock) are smaller in size and weaker in dynamic

pressure than those observed during low IMF cone angles. In particular, these small jets tend to form during high β and M_A conditions.

We presented multi-spacecraft examples of quasi-perpendicular shock crossings during two different solar wind β and M_A conditions, illustrating that when these parameters increase, the shock dynamics change and the shock transition becomes more extended in agreement with previous studies. In particular, we showed the shock transition region exhibits large-amplitude variations not only in the magnetic field and density, but also in dynamic pressure. Earthward magnetosheath jets were consequently found in this transition region. Analyzing one of these in more detail, we found evidence of a gyrating ion population that was significantly contributing to the earthward dynamic pressure. Thus, ion motion near the shock and/or near downstream magnetic structures may lead to jet-like observations. Deeper in the magnetosheath the plasma structuring has dissipated and at least in these particular events we did not see jets there. This indicates that these types of quasi-perpendicular jet-like structures are not expected to be geoeffective. However, they are a part of high β and high M_A shock dynamics, and their relevance may be more significant at shock environments where the magnetic field obliquity, β, and M_A are frequently higher. Future multi-spacecraft studies are needed to clarify the nature of these jets: how they form and how they propagate.

Data Availability Statement

THEMIS and OMNI data can be accessed via, for example, NASA's Coordinated Data Analysis Web (https://cdaweb.gsfc.nasa.gov/). The magnetosheath and jet data set used in this study can be found at Koller et al. (2021).

Acknowledgments
LV acknowledges the financial support of the University of Turku Graduate School. HH and ATL were supported by Royal Society awards URF\R1\180671 and RGF\EA\181090. HH thanks for support by the International Space Science Institute (ISSI) in Bern, through ISSI International Team project #465 "Foreshocks Across The Heliosphere: System Specific Or Universal Physical Processes?." FP is supported by the German Ministerium für Wirtschaft und Klimaschutz and the German Zentrum für Luft- und Raumfahrt under contract 50 OC 2201. We acknowledge NASA contract NAS5-02099 and V. Angelopoulos for use of data from the THEMIS Mission.

References

Angelopoulos, V. (2008). The THEMIS mission. *Space Science Reviews*, *141*(1), 5–34. https://doi.org/10.1007/s11214-008-9336-1

Archer, M. O., & Horbury, T. S. (2013). Magnetosheath dynamic pressure enhancements: Occurrence and typical properties. *Annales Geophysicae*, *31*(2), 319–331. https://doi.org/10.5194/angeo-31-319-2013

Archer, M. O., Horbury, T. S., & Eastwood, J. P. (2012). Magnetosheath pressure pulses: Generation downstream of the bow shock from solar wind discontinuities. *Journal of Geophysical Research*, *117*(A5), 1–13. https://doi.org/10.1029/2011JA017468

Auster, H. U., Glassmeier, K. H., Magnes, W., Aydogar, O., Baumjohann, W., Constantinescu, D., et al. (2008). The THEMIS fluxgate magnetometer. *Space Science Reviews*, *141*(1–4), 235–264. https://doi.org/10.1007/s11214-008-9365-9

Bale, S., Balikhin, M., Horbury, T., Krasnoselskikh, V., Kucharek, H., Möbius, E., et al. (2005). Quasi-perpendicular shock structure and processes. *Space Science Reviews*, *118*(1–4), 161–203. https://doi.org/10.1007/s11214-005-3827-0

Burch, J. L., Moore, T. E., Torbert, R. B., & Giles, B. L. (2016). Magnetospheric multiscale overview and science objectives. *Space Science Reviews*, *199*(1), 5–21. https://doi.org/10.1007/s11214-015-0164-9

Burgess, D., Lucek, E. A., Scholer, M., Bale, S. D., Balikhin, M. A., Balogh, A., et al. (2005). Quasi-parallel shock structure and processes. In G. Paschmann, S. J. Schwartz, C. P. Escoubet, & S. Haaland (Eds.), *Outer magnetospheric boundaries: Cluster results* (pp. 205–222). Springer Netherlands. https://doi.org/10.1007/1-4020-4582-4_7

Burgess, D., Möbius, E., & Scholer, M. (2012). Ion acceleration at the Earth's bow shock. *Space Science Reviews*, *173*(1), 5–47. https://doi.org/10.1007/s11214-012-9901-5

Burgess, D., Wilkinson, W. P., & Schwartz, S. J. (1989). Ion distributions and thermalization at perpendicular and quasi-perpendicular supercritical collisionless shocks. *Journal of Geophysical Research*, *94*(A7), 8783–8792. https://doi.org/10.1029/JA094iA07p08783

Goncharov, O., Gunell, H., Hamrin, M., & Chong, S. (2020). Evolution of high-speed jets and plasmoids downstream of the quasi-perpendicular bow shock. *Journal of Geophysical Research: Space Physics*, *125*(6), e2019JA027667. https://doi.org/10.1029/2019JA027667

Hao, Y., Lembege, B., Lu, Q., & Guo, F. (2016). Formation of downstream high-speed jets by a rippled nonstationary quasi-parallel shock: 2-d hybrid simulations. *Journal of Geophysical Research: Space Physics*, *121*(3), 2080–2094. https://doi.org/10.1002/2015JA021419

Hietala, H., Laitinen, T. V., Andréeová, K., Vainio, R., Vaivads, A., Palmroth, M., et al. (2009). Supermagnetosonic jets behind a collisionless quasiparallel shock. *Physical Review Letters*, *103*(24), 245001. https://doi.org/10.1103/PhysRevLett.103.245001

Hietala, H., & Plaschke, F. (2013). On the generation of magnetosheath high-speed jets by bow shock ripples. *Journal of Geophysical Research: Space Physics*, *118*(11), 7237–7245. https://doi.org/10.1002/2013JA019172

Johlander, A., Schwartz, S. J., Vaivads, A., Khotyaintsev, Y. V., Gingell, I., Peng, I. B., et al. (2016). Rippled quasiperpendicular shock observed by the magnetospheric multiscale spacecraft. *Physical Review Letters*, *117*(16), 165101. https://doi.org/10.1103/PhysRevLett.117.165101

Kajdič, P., Raptis, S., Blanco-Cano, X., & Karlsson, T. (2021). Causes of jets in the quasi-perpendicular magnetosheath. *Geophysical Research Letters*, *48*(13), e2021GL093173. https://doi.org/10.1029/2021GL093173

Karimabadi, H., Roytershteyn, V., Vu, H. X., Omelchenko, Y. A., Scudder, J., Daughton, W., et al. (2014). The link between shocks, turbulence, and magnetic reconnection in collisionless plasmas. *Physics of Plasmas*, *21*(6), 062308. https://doi.org/10.1063/1.4882875

Karlsson, T., Kullen, A., Liljeblad, E., Brenning, N., Nilsson, H., Gunell, H., & Hamrin, M. (2015). On the origin of magnetosheath plasmoids and their relation to magnetosheath jets. *Journal of Geophysical Research: Space Physics*, *120*(9), 7390–7403. https://doi.org/10.1002/2015JA021487

Kennel, C. F., Edmiston, J. P., & Hada, T. (1985). A quarter century of collisionless shock research. In *Collisionless shocks in the heliosphere: A tutorial review* (pp. 1–36). American Geophysical Union (AGU). https://doi.org/10.1029/GM034p0001

King, J., Natalia Papitashvili, G., & ADNET Systems, I. (2023). One min and 5-min solar wind data sets at the Earth's bow shock nose: 4b. High-resolution OMNI data set. Retrieved from https://omniweb.gsfc.nasa.gov/html/omni_min_data.html#4b

King, J. H., & Papitashvili, N. E. (2005). Solar wind spatial scales in and comparisons of hourly wind and ACE plasma and magnetic field data. *Journal of Geophysical Research*, *110*(A2), A02104. https://doi.org/10.1029/2004JA010649

Koller, F., Plaschke, F., Temmer, M., & Preisser, L. (2021). THEMIS local and upstream magnetosheath jet data 2008–2020 [Dataset]. OSF. https://osf.io/6ywjz

Koller, F., Plaschke, F., Temmer, M., Preisser, L., Roberts, O. W., & Vörös, Z. (2023). Magnetosheath jet formation influenced by parameters in solar wind structures. *Journal of Geophysical Research: Space Physics*, *128*(4), e2023JA031339. https://doi.org/10.1029/2023JA031339

Koller, F., Temmer, M., Preisser, L., Plaschke, F., Geyer, P., Jian, L. K., et al. (2022). Magnetosheath jet occurrence rate in relation to CMEs and SIRs. *Journal of Geophysical Research: Space Physics*, *127*(4), e2021JA030124. https://doi.org/10.1029/2021JA030124

LaMoury, A. T., Hietala, H., Plaschke, F., Vuorinen, L., & Eastwood, J. P. (2021). Solar wind control of magnetosheath jet formation and propagation to the magnetopause. *Journal of Geophysical Research: Space Physics*, *126*(9), e2021JA029592. https://doi.org/10.1029/2021JA029592

Lowe, R. E., & Burgess, D. (2003). The properties and causes of rippling in quasi-perpendicular collisionless shock fronts. *Annales Geophysicae*, *21*(3), 671–679. https://doi.org/10.5194/angeo-21-671-2003

Madanian, H., Desai, M. I., Schwartz, S. J., Wilson, L. B., Fuselier, S. A., Burch, J. L., et al. (2021). The dynamics of a high Mach number quasi-perpendicular shock: MMS observations. *The Astrophysical Journal*, *908*(1), 40. https://doi.org/10.3847/1538-4357/abcb88

McFadden, J. P., Carlson, C. W., Larson, D., Ludlam, M., Abiad, R., Elliott, B., et al. (2008). The THEMIS ESA plasma instrument and in-flight calibration. *Space Science Reviews*, *141*(1–4), 277–302. https://doi.org/10.1007/s11214-008-9440-2

McKean, M. E., Omidi, N., & Krauss-Varban, D. (1995). Wave and ion evolution downstream of quasi-perpendicular bow shocks. *Journal of Geophysical Research*, *100*(A3), 3427–3437. https://doi.org/10.1029/94JA02529

McKean, M. E., Omidi, N., & Krauss-Varban, D. (1996). Magnetosheath dynamics downstream of low Mach number shocks. *Journal of Geophysical Research*, *101*(A9), 20013–20022. https://doi.org/10.1029/96JA01461

Merka, J., Szabo, A., Slavin, J. A., & Peredo, M. (2005). Three-dimensional position and shape of the bow shock and their variation with upstream Mach numbers and interplanetary magnetic field orientation. *Journal of Geophysical Research*, *110*(A4), 1–13. https://doi.org/10.1029/2004JA010944

Ofman, L., & Gedalin, M. (2013). Two-dimensional hybrid simulations of quasi-perpendicular collisionless shock dynamics: Gyrating downstream ion distributions. *Journal of Geophysical Research: Space Physics*, *118*(5), 1828–1836. https://doi.org/10.1029/2012JA018188

Omidi, N., Desai, M., Russell, C. T., & Howes, G. G. (2021). High Mach number quasi-perpendicular shocks: Spatial versus temporal structure. *Journal of Geophysical Research: Space Physics*, *126*(9), e2021JA029287. https://doi.org/10.1029/2021JA029287

Palmroth, M., Hietala, H., Plaschke, F., Archer, M., Karlsson, T., Blanco-Cano, X., et al. (2018). Magnetosheath jet properties and evolution as determined by a global hybrid-Vlasov simulation. *Annales Geophysicae*, *36*(5), 1171–1182. https://doi.org/10.5194/angeo-36-1171-2018

Petrukovich, A. A., & Chugunova, O. M. (2021). Detailed structure of very high-β Earth bow shock. *Journal of Geophysical Research: Space Physics*, *126*(8), e2020JA029004. https://doi.org/10.1029/2020JA029004

Plaschke, F., Hietala, H., & Angelopoulos, V. (2013). Anti-sunward high-speed jets in the subsolar magnetosheath. *Annales Geophysicae*, *31*(10), 1877–1889. https://doi.org/10.5194/angeo-31-1877-2013

Plaschke, F., Hietala, H., Angelopoulos, V., & Nakamura, R. (2016). Geoeffective jets impacting the magnetopause are very common. *Journal of Geophysical Research: Space Physics*, *121*(4), 3240–3253. https://doi.org/10.1002/2016JA022534

Plaschke, F., Hietala, H., Archer, M., Blanco-Cano, X., Kajdič, P., Karlsson, T., et al. (2018). Jets downstream of collisionless shocks. *Space Science Reviews*, *214*(5), 81. https://doi.org/10.1007/s11214-018-0516-3

Plaschke, F., Hietala, H., & Vörös, Z. (2020). Scale sizes of magnetosheath jets. *Journal of Geophysical Research: Space Physics*, *125*(9), e2020JA027962. https://doi.org/10.1029/2020JA027962

Pollock, C., Moore, T., Jacques, A., Burch, J., Gliese, U., Saito, Y., et al. (2016). Fast plasma investigation for magnetospheric multiscale. *Space Science Reviews*, *199*(1), 331–406. https://doi.org/10.1007/s11214-016-0245-4

Raptis, S., Karlsson, T., Plaschke, F., Kullen, A., & Lindqvist, P.-A. (2020). Classifying magnetosheath jets using MMS: Statistical properties. *Journal of Geophysical Research: Space Physics*, *125*(11), e2019JA027754. https://doi.org/10.1029/2019JA027754

Raptis, S., Karlsson, T., Vaivads, A., Lindberg, M., Johlander, A., & Trollvik, H. (2022). On magnetosheath jet kinetic structure and plasma properties. *Geophysical Research Letters*, *49*(21), e2022GL100678. https://doi.org/10.1029/2022GL100678

Raptis, S., Karlsson, T., Vaivads, A., Pollock, C., Plaschke, F., Johlander, A., et al. (2022). Downstream high-speed plasma jet generation as a direct consequence of shock reformation. *Nature Communications*, *13*(1), 598. https://doi.org/10.1038/s41467-022-28110-4

Scholer, M., Fujimoto, M., & Kucharek, H. (1993). Two-dimensional simulations of supercritical quasi-parallel shocks: Upstream waves, downstream waves, and shock re-formation. *Journal of Geophysical Research*, *98*(A11), 18971–18984. https://doi.org/10.1029/93JA01647

Schwartz, S. J. (1991). Magnetic field structures and related phenomena at quasi-parallel shocks. *Advances in Space Research*, *11*(9), 231–240. https://doi.org/10.1016/0273-1177(91)90039-M

Shue, J.-H., Song, P., Russell, C. T., Steinberg, J. T., Chao, J. K., Zastenker, G., et al. (1998). Magnetopause location under extreme solar wind conditions. *Journal of Geophysical Research*, *103*(A8), 17691–17700. https://doi.org/10.1029/98JA01103

Sulaiman, A. H., Masters, A., Dougherty, M. K., Burgess, D., Fujimoto, M., & Hospodarsky, G. B. (2015). Quasiperpendicular high Mach number shocks. *Physical Review Letters*, *115*(12), 125001. https://doi.org/10.1103/PhysRevLett.115.125001

Sundberg, T., Burgess, D., Scholer, M., Masters, A., & Sulaiman, A. H. (2017). The dynamics of very high Alfvén Mach number shocks in space plasmas. *The Astrophysical Journal Letters*, *836*(1), L4. https://doi.org/10.3847/2041-8213/836/1/L4

Suni, J., Palmroth, M., Turc, L., Battarbee, M., Johlander, A., Tarvus, V., et al. (2021). Connection between foreshock structures and the generation of magnetosheath jets: Vlasiator results. *Geophysical Research Letters*, *48*(20), e2021GL095655. https://doi.org/10.1029/2021GL095655

Tinoco-Arenas, A., Kajdič, P., Preisser, L., Blanco-Cano, X., Trotta, D., & Burgess, D. (2022). Parametric study of magnetosheath jets in 2D local hybrid simulations. *Frontiers in Astronomy and Space Sciences*, *9*. https://doi.org/10.3389/fspas.2022.793195

Vokhmyanin, M. V., Stepanov, N. A., & Sergeev, V. A. (2019). On the evaluation of data quality in the OMNI interplanetary magnetic field database. *Space Weather*, *17*(3), 476–486. https://doi.org/10.1029/2018SW002113

Vuorinen, L., Hietala, H., & Plaschke, F. (2019). Jets in the magnetosheath: IMF control of where they occur. *Annales Geophysicae*, *37*(4), 689–697. https://doi.org/10.5194/angeo-37-689-2019

Walsh, B. M., Bhakyapaibul, T., & Zou, Y. (2019). Quantifying the uncertainty of using solar wind measurements for geospace inputs. *Journal of Geophysical Research: Space Physics*, *124*(5), 3291–3302. https://doi.org/10.1029/2019JA026507